© 2018. Published by The Company of Biologists Ltd | Journal of Experimental Biology (2018) 221, jeb178897. doi:10.1242/jeb.178897

RESEARCH ARTICLE

Global dynamics of bipedal macaques during grounded and aerial running

Reinhard Blickhan[1,*], Emanuel Andrada[2], Eishi Hirasaki[3] and Naomichi Ogihara[4,5]

ABSTRACT

Macaques trained to perform bipedally use grounded running, skipping and aerial running, but avoid walking. The preference for grounded running across a wide range of speeds is substantially different from the locomotion habits observed in humans, which may be the result of differences in leg compliance. In the present study, based on kinematic and dynamic observations of three individuals crossing an experimental track, we investigated global leg properties such as leg stiffness and viscous damping during grounded and aerial running. We found that, in macaques, similar to human and bird bipedal locomotion, the vector of the ground reaction force is directed from the center of pressure (COP) to a virtual pivot point above the center of mass (COM). The visco-elastic leg properties differ for the virtual leg (COM-COP) and the effective leg (hip-COP) because of the position of the anatomical hip with respect to the COM. The effective leg shows damping in the axial direction and positive work in the tangential component. Damping does not prevent the exploration of oscillatory modes. Grounded running is preferred to walking because of leg compliance. The transition from grounded to aerial running is not accompanied by a discontinuous change. With respect to dynamic properties, macaques seem to be well placed between bipedal specialists (humans and birds). We speculate that the losses induced in the effective leg by hip placement and slightly pronograde posture may not pay off by facilitating stabilization, making bipedal locomotion expensive and insecure for macaques.

KEY WORDS: Macaque locomotion, Leg stiffness, Leg damping, Leg work, Gait

INTRODUCTION

Macaques trained to perform bipedally routinely use bipedal locomotion with ease (Nakatsukasa et al., 2006). Regular training leads to adaptations to bipedal locomotion (Hayama et al., 1992), such as human-like lumbar lordosis and more robust femora (Nakatsukasa and Hayama, 1991). However, the skeletal system of the macaque is certainly more similar to that of ordinary monkeys and lacks the substantial morphological adaptations to bipedalism observed in the human skeletal system. The range of hip joint extension is more restricted in macaques than in humans owing to architectural differences in the muscles and fascia connecting the pelvis and thigh (Ogihara et al., 2007). Compared with human feet, macaque feet are much more biased towards gripping and climbing. We expect that such adaptations influence global leg properties and, consequently, the global dynamics of locomotion. Compared with that of humans, the locomotor system of the macaque is less well adapted to bipedal locomotion. Even trained macaques still prefer quadrupedal locomotion unless required; for example, while reaching for food or carrying loads manually. In our experiments, bipedal locomotion was stimulated by rewards. The macaques freely selected speed and gait, but in our recent study, we did not identify even a single pendular walk (Ogihara et al., 2018). In contrast to adult humans, macaques prefer grounded running, skipping and aerial running.

Focusing on the global dynamics of locomotion reduces the number of descriptive parameters and facilitates comparisons across a wide range of bipedal species. It also allows us to answer the question whether the transitions from grounded to aerial running and from walking to aerial running are reflected in the speed dependencies of one or a few parameters such as global leg properties**.** Moreover, it allows us to interrelate the experimental results with dynamic simulations based on lumped parameter models such as the spring–mass model. Referring to lumped parameter models of running gaits, we first think of the simple spring–mass model or the spring-loaded inverted pendulum (SLIP; Blickhan, 1989) model, in which a virtual leg connects the center of mass (COM) to the center of pressure (COP) at the contacting foot (Fig. 1A). As all external forces accelerate the COM, this yields a decent description of the 'global dynamics' of the COM for human aerial running. However, detailed investigations have shown that, especially during walking, the vector of the ground reaction force does not point to the COM but to the virtual pivot point (VPP), cranial to the COM (Fig. 1A; Maus et al., 2010; Müller et al., 2017). The VPP corresponds to the metacenter of a ship and acts as though the system would be suspended at the VPP. With the COM below the VPP, the angular momentum of the system is stabilized. A VPP has been identified during locomotion in bipeds and quadrupeds and is even maintained in the presence of human walking with bent posture (Müller et al., 2017). The SLIP model only describes the contribution of the component of the forces directed to the COM, i.e. axial with respect to the virtual leg. During human aerial running with a vanishing height of the VPP above the COM, this approximation delivers useful results. Similarly, using the effective leg, i.e. the leg connecting the hip to the COP (Fig. 1A), calculating lumped parameters such as leg stiffness results in only minor deviations from descriptions of the virtual leg, as the human hip is located roughly below and not far from the COM. Systematic comparisons of both descriptions, i.e. virtual and effective legs, for human walking and aerial running are missing. Investigations on grounded running in birds (Andrada et al., 2013, 2014; Blickhan et al., 2015) have shown that a hip position far posterior to the

[1]Science of Motion, Friedrich-Schiller-University, 07749 Jena, Germany. [2]Institute of Zoology and Evolutionary Research, Friedrich-Schiller University, 07743 Jena, Germany. [3]Primate Research Institute, Kyoto University, Inuyama, Aichi 484-8506, Japan. [4]Department of Mechanical Engineering, Keio University, 3-14-1 Hiyoshi, Kohoku-ku, Yokohama 223-8522, Japan. [5]Department of Biological Science, Graduate School of Science, The University of Tokyo, 7-3-1 Hongo, Bunkyo-ku, Tokyo 113-0033, Japan.

*Author for correspondence (reinhard.blickhan@uni-jena.de)

R.B., 0000-0001-6751-5621; E.A., 0000-0002-9300-4056; N.O., 0000-0002-1697-9263

Received 5 February 2018; Accepted 15 October 2018

Journal of Experimental Biology (2018) 221, jeb178897. doi:10.1242/jeb.178897

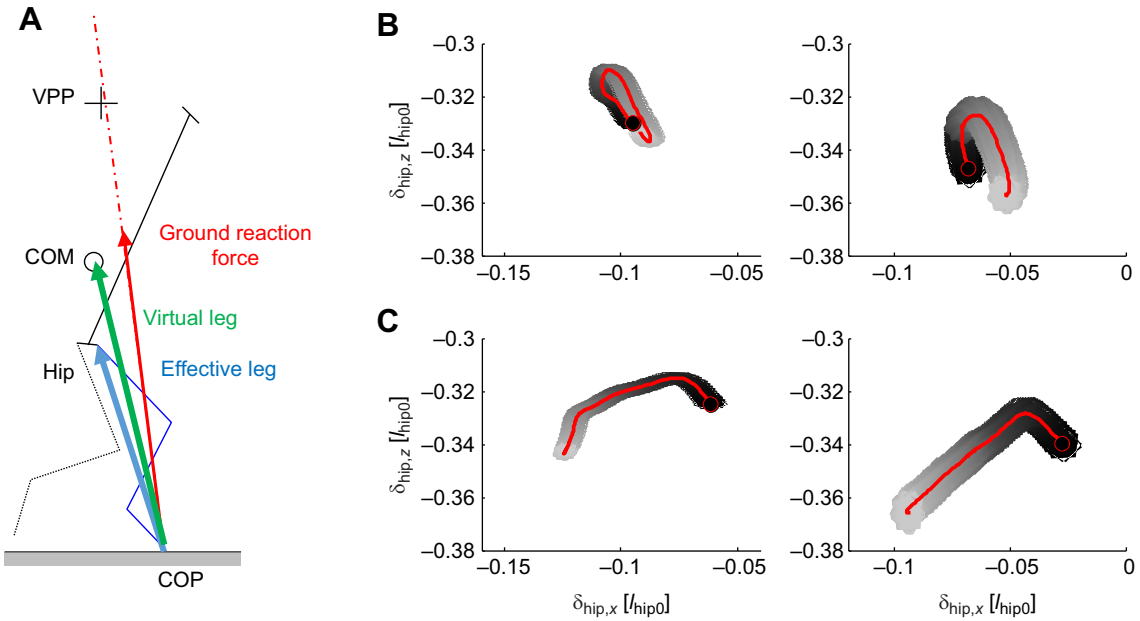

Fig. 1. Locations, leg types, and displacement of the hip. (A) Points, legs and force. Stick figure with the virtual pivot point (VPP), center of mass (COM) and hip marked. The effective leg (blue arrow) points from the center of pressure (COP) to the hip, and the virtual leg (green arrow) points from the COP to the COM. The ground reaction force (red arrow) is directed close to the VPP. (B,C) Sagittal displacement (δ_{hip} normalized to effective leg length l_{hip0}) of the mid hip (B) and the hip of the loaded leg (C) with respect to the COM during contact. Left: grounded running; right: aerial running. Black circle: touchdown. Shaded area: standard error (s.e.) in the horizontal (*x*) and vertical directions (*z*); it changes with time from black to gray.

COM results in an effective leg entailing strong damping. Correspondingly, the lumped parameter model should include viscous elements to describe the resulting dynamics. Birds are well adapted to bipedal locomotion. Traditionally, the caudal position of the hip in birds is attributed to flight. However, many extant species and many ancestors are flightless, and ongoing studies by one of the authors (E.A.) support the fact that the pronograde posture in birds facilitates stabilization. In macaques, the hip also seems to be positioned farther from the COM compared with that in humans. Correspondingly, we expect that the macaque leg deviates from purely elastic behavior and that differences exist between the virtual and effective legs.

To gain a better understanding of why macaques prefer grounded running to pendular walking, in the present study, we aimed to evaluate the global stiffness of the leg during bipedal locomotion in macaques. We also investigated whether visco-elastic and non-axial contributions are significant in the description of leg properties and whether they hamper explorations of resilience. Moreover, as macaques still prefer to walk quadrupedally, we investigated whether their ability to control the direction of the ground reaction force during bipedal locomotion might be limited.

MATERIALS AND METHODS

Animals

Three regularly trained performing macaques, *Macaca fuscata* Blyth 1875, from the Suo Monkey Performance Association (Kumamoto, Japan) participated in the experiment. The macaques (Ku, Po and Fu) were all adult males (age: 15, 13, 12 years; mass: 8.64, 8.81, 8.79 kg, respectively) that had been trained for bipedal walking and performing since the age of about 1 year. The grand mean leg lengths between those at touchdown and takeoff were 0.399, 0.339 and 0.405 m for the effective leg (l_{hip0}) and 0.529, 0.465 and 0.520 m for the virtual leg (l_{COM0}), respectively.

Setup

The macaques ran across a flat wooden track (length: 5 m) with two embedded force plates. Kinematics and ground reaction forces were captured with an eight-camera infrared motion-capture system (Oqus 3+, Qualisys, Göteborg, Sweden) and force plates (EPF-S-1.5KNSA13; Kyowa Dengyo, Tokyo), respectively, at a rate of 200 frames or samples per second. Details of the experimental setup and procedure are provided in Ogihara et al. (2018).

Procedure

An individual coach and caregiver prevented the animals from escaping with the use of a slack leash. A total of 15 markers were placed at the acromion, sternum xiphoid, tenth thoracic vertebra, anterior superior iliac spine, sacrum, greater trochanter, lateral epicondyle, lateral malleolus and fifth metatarsal head of each participating animal. Static trials were used to estimate the medial joint positions (medial epicondyle, medial malleolus and second metatarsal head).

Ethical statement

The experiments were approved by the Animal Welfare and Animal Care Committee, Primate Research Institute, Kyoto University. All institutional guidelines were followed for this study. The macaques were easily motivated to walk bipedally using a reward system. The bipedal walking speed was freely selected and the experiments were stopped when any signs of unwillingness were observed.

Data evaluation

Dropouts in the kinematic data of fewer than 11 frames were interpolated linearly and low-pass filtered using a zero-phase fifth-order Butterworth filter. Joint centers of the knee, ankle and metatarsals were calculated by projecting the half-distance of the medial and lateral markers from the lateral markers perpendicular to the main plane of movement of the knee. The location of the hip was

estimated as a projection perpendicular to the main plane of movement of the knee from the greater trochanter marker using the distance obtained from cadaver measurement (Ogihara et al., 2009). From this, the position of the segmental COM could be obtained using morphometric data (Ogihara et al., 2011). The COM of the trunk is located on the line connecting the mid-hip joint (midpoint of the left and right joint centers) and mid-shoulder. However, to account for the difference in trunk posture between the cadaver specimen used in the whole-body computed tomography investigation and the macaques during locomotion, we horizontally shifted the COM position based on the assumption of zero mean momentum with respect to the COM during the stance phase. A shift of the tarsal markers with respect to the COP was therefore added (net correction in millimeters: grounded running: Ku −53, Fu −62 and Po −50; aerial running: Ku −57, Fu −60 and Po −72; parameters with reference to the position of the COM were sensitive to this correction; see Discussion). Within a presentation of the ground reaction forces with respect to the instantaneous COM (COM-fixed coordinate system), the VPP was calculated as the center of the waist (minimum horizontal width) established by crossing the extended ground reaction force vectors (first and last 10% of contact time omitted).

In the present study, smooth gait sequences without stumbling and distraction were selected for further analysis. These were classified as a symmetrical grounded run for duty factor ≥0.5 or a symmetrical aerial run for duty factor <0.5. The selections resulted in a sample of 76 (Ku: 32; Fu: 42; Po: 2) trials for grounded running and 20 (Ku: 14; Fu: 2; Po: 4) trials for aerial running. We focused on leg mechanical properties in the stance phase.

Trunk angle β and leg angle α were calculated with respect to the vertical axis and were positive for clockwise rotations (forward tilt). Force tracings were filtered using a sixth-order Savitzky–Golay filter across 16 samples. The threshold for determining the instant of touchdown and takeoff from the vertical force recordings was 0.05 [mg].

The macaques' global dynamics changed with speed during bipedal locomotion. Froude speed v_{Fr} was defined as $v/\sqrt{(gl_{\mathrm{hip0}})}$, with g being the gravitational acceleration and l_{hip0} being the mean of the touchdown and takeoff lengths of the effective leg. To calculate stiffness and damping, a parallel arrangement of a linear spring and damper was assumed (Kelvin–Voigt model; see Andrada et al., 2014). Both coefficients were obtained by a bilinear fit in which the leg lengthening $\Delta l(t)=[l(t)-l_0]$ and leg shortening velocity $\dot{l}(t)$ were given from the measurements as independent variables, and the force $F(t)$ was given as the dependent variable:

$$F(t) = k \cdot \Delta l(t) + D \cdot \dot{l}(t). \quad (1)$$

To facilitate comparison between animals of different sizes, we implemented the dimensionless formula:

$$\hat{F}(\hat{t}) = \hat{k} \cdot \widehat{\Delta l}(\hat{t}) + \hat{D} \cdot \frac{\mathrm{d}\widehat{\Delta l}(\hat{t})}{\mathrm{d}\hat{t}}, \quad (2)$$

with

$$\hat{F} = \frac{F(t)}{mg},\ \hat{l} = \frac{l}{l_0},\ \widehat{\Delta l} = \frac{\Delta l}{l_0} \text{ and } \hat{t} = t\sqrt{\frac{g}{l_0}}.$$

Based on a comparison of the literature, the influence of the selected l_0 must be considered as it strongly affects the outcome of the stiffness calculations. By replacing l_0 with γl_0, the equation used to obtain dimensionless stiffness and damping by fitting $\hat{F}(\widehat{\Delta l}, (\mathrm{d}\widehat{\Delta l}/\mathrm{d}\hat{t}))$ results in:

$$\hat{F} = \frac{\hat{k}}{\gamma}\left(\frac{l}{l_0} - 1\right) + \frac{\hat{k}}{\gamma}(1-\gamma) + \frac{\hat{D}}{\sqrt{\gamma}}\frac{\mathrm{d}\hat{l}}{\mathrm{d}\hat{t}}.$$

For γ=1.2, a damping coefficient of 1 changes to 0.91; however, a stiffness of 15 diminishes to 10. We calculated l_0 in each trial as the mean of the touchdown and takeoff lengths. This implies that for a leg shorter at touchdown than at takeoff, the leg spring is compressed at touchdown ($l<l_0$), but stretched ($l>l_0$) at takeoff, or vice versa for a leg longer at touchdown than at takeoff.

For completeness and to enhance compatibility with the recent literature (Aminiaghdam et al., 2017), a series model (Maxwell model) was fitted to our data. The length and force of the model with the damper (index D) in series with the spring (index S) was calculated as $l=l_D+l_S$ and $F=F_D=F_S$, respectively. As:

$$l_D = \int_0^t \dot{l}_D \mathrm{d}t + l_{D0} = \frac{1}{D}\int_0^t F\mathrm{d}t + l_{D0} \text{ and } F = k(l_{s0} - l + l_D),$$

$$F = k(l_0 - l) + \frac{k}{D}\int_0^t F\mathrm{d}t,$$

assuming $l_{S0}=l_{D0}=l_0/2$. In dimensionless form:

$$\hat{F}(\hat{t}) = \hat{k}(1 - \hat{l}(\hat{t})) - \frac{\hat{k}}{\hat{D}}\int_0^{\hat{t}} \hat{F}(\hat{t})\mathrm{d}\hat{t}, \quad (3)$$

where $\hat{F}(\hat{t})$, $\hat{l}(\hat{t})$ and $\int_0^{\hat{t}} \hat{F}(\hat{t})\mathrm{d}\hat{t}$ were obtained from the data. Stiffness and damping were estimated using a non-linear fit. We limited calculations to $\hat{D} < 1000$. For high resilience, the stiffness in the two models converged. In this case, damping approached 0 in the Kelvin–Voigt model, whereas it approached infinity in the Maxwell model. As our results were clustered around the pure elastic situation, the mean values calculated using the Maxwell model were not useful. Here, we only present the results for the Kelvin–Voigt model. Within each gait, both situations with damping, i.e. with axial energy dissipation and axial net work generation, were observed. To facilitate reading, we defined damping being positive for the case of energy dissipation and negative for the case of increased net work generation.

Dimensionless work (normalized to mgl_0) generated by the leg from touchdown (TD) to takeoff (TO), $\hat{W}_{\mathrm{leg}}$, was calculated as:

$$\hat{W}_{\mathrm{leg}} = \hat{W}_{\mathrm{ax}} + \hat{W}_{\mathrm{tan}} = \int_{\mathrm{TD}}^{\mathrm{TO}} \hat{F}_{\mathrm{ax}}\mathrm{d}\hat{l} + \int_{\mathrm{TD}}^{\mathrm{TO}} \hat{l}\,\hat{F}_{\mathrm{tan}}\mathrm{d}\alpha\ , \quad (4)$$

where $\hat{W}_{\mathrm{ax}}$ is dimensionless axial work, $\hat{W}_{\mathrm{tan}}$ is tangential work, $\hat{F}_{\mathrm{ax}}$ is dimensionless axial force, $\hat{F}_{\mathrm{tan}}$ is dimensionless tangential force, $\hat{l}$ is dimensionless leg length and α is the angle of attack of the leg with respect to the vertical axis.

The above parameters were calculated for both the virtual and effective legs connecting the COM and COP and the hip joint and COP, respectively.

Translational work of the COM was calculated as:

$$\hat{W}_{\mathrm{hor}} = \int_{\mathrm{TD}}^{\mathrm{TO}} \hat{F}_x\mathrm{d}\hat{x} \text{ and } \hat{W}_{\mathrm{vert}} = \int_{\mathrm{TD}}^{\mathrm{TO}} (\hat{F}_z - 1)\mathrm{d}\hat{z}, \quad (5)$$

with the horizontal coordinate x and the vertical coordinate z. This estimate was independent of leg models and COM position.

Trials were selected with respect to the symmetry of the stepping pattern. Mean accelerations within the trials obtained from horizontal forces were below ±0.08 [g] {grounded running: (−0.008±0.030s.d.) [g]; aerial running: (−0.028±0.028s.d.) [g]}. Bilinear extrapolation with respect to horizontal and vertical acceleration to correct for unsteady effects did not result in significant differences (P>0.3) for D_{hip}, $W_{ax,hip}$ or $W_{tan,hip}$ during grounded running. Higher correlations and significantly different estimates (marked with ∼) were achieved with bilinear regressions based on the horizontal and vertical components of translational work.

The circumflex to indicate dimensionless quantities is only used within equations (see above and Discussion). In the text, quantities are given in the units generating the dimensionless number. Thus, instead of $\hat{l}_{COM}$, we use l [l_{COM0}] for the dimensionless length of the virtual leg or we provide the mean value (±s.d.) of the lengths considered and its units, such as (0.18±0.13s.d.) [l_{COM0}]. This keeps the reader aware of the particular definition anywhere in the text. For quantities in SI units presented in the text or captions, square brackets are omitted.

Custom software was written in MATLAB 14 (MathWorks, Natick, MA, USA). Part of the statistics was analyzed using IBM SPSS 23 (IBM, Armonk, NY, USA). Comparisons between means were done after checking for normal distributions (KS-test) either with the Wilcoxon test and dependent Student's t-test or, in the case of independent samples, with the Mann–Whitney U-test or independent Student's t-test (sample size: grounded running n=76, aerial running n=20; not significant: P>0.05; in the case of multiple comparisons, the Bonferroni correction was used).

RESULTS

The global visco-elastic properties of the virtual and effective legs of macaques during grounded and aerial running were found to change continuously without abrupt discontinuities in mechanical parameters across the speed marking a gait transition.

Kinematic references – hip and COM

The property difference between the effective and virtual leg depended on the behavior of the hip with respect to the COM. The hip of the loaded leg was below and behind the COM (grand mean: Dx: −0.104 [l_{hip0}] and −0.067 [l_{hip0}]; Dz: −0.33 [l_{hip0}] and −0.35 [l_{hip0}] for grounded and aerial running, respectively; Fig. 1C). In the horizontal direction (x), the hip was close to the estimated COM. The spread in the horizontal direction of about 0.06 [l_{hip0}] was largely the result of pelvic rotation; this includes the counteracting effect {ca. 0.02 [l_{hip0}]; Fig. 1B} owing to the minor pitching movement of the trunk.

Posture and kinematics of global legs

The time course of the trunk angle β (Fig. 2A) indicated minor forward tilt during loading and backward tilt during unloading. Total amplitudes (Table 1) were similar during grounded and aerial running. The extension phase developed earlier during running and the posture was slightly more erect compared with grounded running, and was significantly more erect (P<0.007) at takeoff than at touchdown, especially during aerial running.

The leg retracted at a constant rate marginally disturbed by the impact phase (Fig. 2B). During aerial running, rotation was shifted significantly to the unloading side (P<0.001). Slightly smaller angles (P<0.006) with the same tendency were documented for the virtual leg versus the effective leg. Differences between grounded and aerial running were not significant for touchdown. Angles at takeoff were significantly larger for the virtual leg (P<0.001). Differences between touchdown and takeoff and between the effective and virtual leg were all highly significant (P<0.001).

Compression of the axial leg (Fig. 2C) was more pronounced during aerial compared with grounded running, corresponding to the increase in the ground reaction force. For the effective leg, slight net shortening was observed during grounded running and net lengthening was observed during aerial running. For the virtual leg, net lengthening was observed during grounded running and even enhanced during aerial running (P<0.001). Compression was larger during aerial compared with grounded running and larger for the effective than for the virtual leg (P<0.006).

Force and COP

Registration of ground reaction force and the COP represent the dynamic basis for the estimation of global leg properties. Ground reaction forces observed during grounded running and aerial running differed only little (Fig. 2D). The vertical component consisted of an initial impact phase followed by a single positively skewed active peak (Ogihara et al., 2007, 2010). The active peak amplitude was significantly larger during aerial running (1.58±0.10s.d.) [mg] compared with that during grounded running (1.35±0.14s.d.) [mg] (P<0.001). Skew was significantly higher during grounded running (0.33±0.05s.d.) than during aerial running (0.26±0.05s.d.) (P<0.001). The horizontal force showed deceleration and acceleration phases. The maximum in the acceleration phase observed during aerial running was slightly enhanced compared with that during grounded running (P<0.001).

The time courses of the foot loading indicated by the COP (Fig. 2E) were also very similar (P>0.16) during grounded and aerial running. During the loading phase, the COP moved posteriorly (−0.07±0.05s.d.) [l_{hip0}] and then continuously anteriorly (0.20±0.05s.d.) [l_{hip0}] to the tip of the foot.

Direction of reaction forces – combining dynamics and kinematics

The dependency of the length of the vector of the ground reaction force on time in the examples presented in Fig. 3 mirrors the mean values of the components documented in Fig. 2D. An impact within the first 20% of contact was followed by an active peak reaching its maximum at about 31% for grounded running and 38% for aerial running. Because of the low vertical momentum, the leveling off of the force and the short double support, the elevation of the COM decreased during contact in both grounded and aerial running. The ground reaction forces were directed toward a point above the COM, the VPP (Figs 1A, 3). During grounded running, the mean height of the VPP above the COM was (0.38±0.16s.d.) [l_{hip0}] and was significantly higher (P<0.001) than the value observed during aerial running (0.20±0.10s.d.) [l_{hip0}]. The height of the VPP diminished with speed (Fig. 4).

Global parameters

Dimensionless stiffness and damping depended on speed and differed for the effective and virtual legs. The values obtained for aerial running were within the tendencies obtained for grounded running (Figs 5 and 6).

The mean dimensionless stiffness (Table 2) of both the effective and virtual legs was similar between grounded and aerial running. The stiffness estimates obtained with the bilinear fit (visco-elastic model) correlated highly (R>0.85; P<0.001) with stiffness obtained from the ratio of peak force and maximum leg shortening, and with

Journal of Experimental Biology (2018) 221, jeb178897. doi:10.1242/jeb.178897

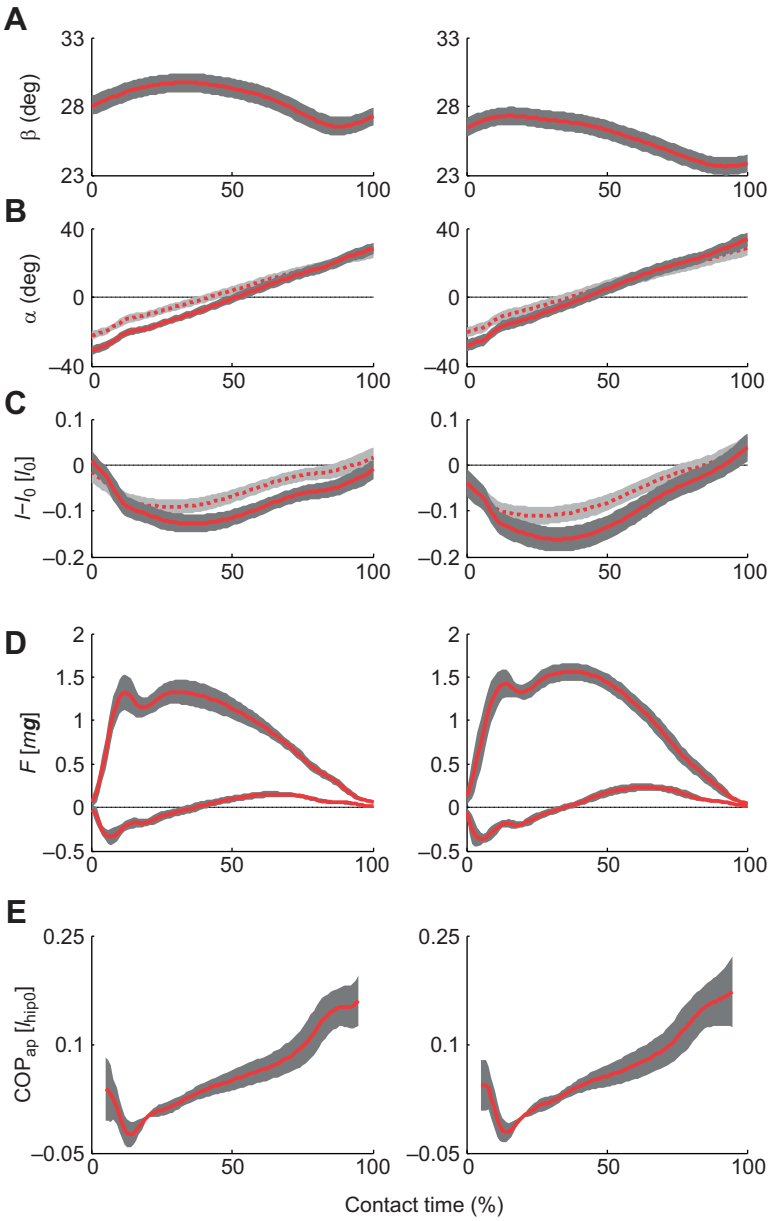

Fig. 2. Changes in dynamic and kinematic parameters (mean±s.d.) with contact time (t_c) for grounded running (left) and aerial running (right). (A) Trunk angle (β). (B) Leg angle (α). (C) Axial compression of the leg ($l–l_0$). Dashed lines and light gray shading in B and C: virtual leg (normalized to virtual leg length l_{COM0}); continuous lines and dark gray shading: effective leg (normalized to effective leg length l_{hip0}). (D) Vertical and anteroposterior components of the ground reaction force. (E) Anteroposterior component of the COP. COP at 20% contact time (t_c) set to 0 and the first and last 5% are omitted.

values obtained by a simple linear fit. Corresponding mean values differed only slightly {absolute difference <0.7 [mg/l_0]; effective leg: P<0.009; virtual leg: P>0.21}.

For the effective leg during grounded running, mean damping (Table 2) was positive, indicating counter-clockwise force–length loops (Fig. 5A, left) and absorption. During aerial running (Fig. 5B, left), the damping was not significantly different from zero. For the virtual leg (Fig. 5C,D), damping was lower for aerial than for grounded running and negative in both gaits.

Dimensionless stiffness increased with Froude speed for the effective leg (Fig. 6A, left; for regression equations, see Fig. 6 caption). The correlation was not significant for the virtual leg. Damping of the effective leg (Fig. 6A, right) decreased to reach negative values, i.e. force–length loops for aerial running (Fig. 5B). This tendency was even stronger for the virtual leg (Fig. 6B, right), indicating clockwise loops for grounded running (Fig. 5C). All loops for aerial running were clockwise. The stiffness values obtained by the classical approach (peak vertical ground reaction force/peak shortening) were largely reproduced by fitting the visco-elastic model. Compared with stiffness, damping depended more on Froude speed (Fig. 6, right), especially and unexpectedly for the virtual leg. Similar to the stiffness values within the observed variance, the values observed for aerial running followed the same regression as those for grounded running.

The values with correction (Table 2; see 'Work', below) did not differ significantly (P>0.095) from those without correction, with the exception of damping (P<0.001) of the effective leg (D_{hip}). The corrected damping coefficients obtained for aerial running were not significantly different from zero.

Work

Integration of the work loops allows for an estimation of energetics independent of descriptive simplifying models. During grounded running, the mean axial work (Table 2) of the effective leg indicated absorption or counterclockwise work loops, whereas during aerial running, the mean axial work did not differ from zero. Net tangential work of the effective leg was observed during both grounded and aerial running.

Journal of Experimental Biology (2018) 221, jeb178897. doi:10.1242/jeb.178897

Table 1. Kinematic parameters for grounded running and aerial running

Variable		Grounded running (mean±s.d.)	Aerial running (mean±s.d.)	*P* (GR/R)
β (deg)	TD	28.1±6.4	26.5±3.1	0.580
	TO	27.2±5.5	23.9±2.9	0.031
	Range	3.9±1.5	3.9±1.3	1.000
	Max.	30.0±5.9	27.4±2.9	0.130
	%	43.0±22.2	18.0±8.1	0.000
α_{hip} (deg)	TD	−31.0±2.5	−28.3±3.3	0.002
	TO	28.2±3.5	33.4±4.1	0.000
	Range	59.4±3.9	61.7±3.7	0.065
α_{COM} (deg)	TD	−22.2±2.3	−20.5±2.9	0.071
	TO	26.0±3.3	28.6±4.5	0.005
	Range	48.2±3.2	49.1±3.7	0.515
l_{hip} [l_{hip0}]	TD	1.01±0.02	0.96±0.02	0.000
	TO	0.99±0.02	1.04±0.02	0.000
	Range	0.15±0.02	0.20±0.05	0.000
	Min.	0.87±0.02	0.84±0.03	0.000
	%	36.88±4.03	33.20±2.79	0.001
l_{COM} [l_{COM0}]	TD	0.99±0.02	0.96±0.02	0.000
	TO	1.01±0.02	1.04±0.02	0.000
	Range	0.12±0.03	0.15±0.04	0.000
	Min.	0.91±0.02	0.89±0.02	0.000
	%	28.68±5.89	25.40±3.89	0.064

β, trunk angle; α_{hip} and α_{COM}, leg angles of the effective and virtual legs; l_{hip} and l_{COM}, lengths of the effective and virtual legs. Properties are given at touchdown (TD) and takeoff (TO), range and extremum (see Fig. 2), and % time of occurrence within contact. GR/R: significance of differences between grounded and aerial running.

For the virtual leg during grounded running, the axial net work was positive for grounded and aerial running, with the exception of the insignificant tangential work obtained during aerial running.

For the effective leg, separate descriptions of the axial and tangential work observed during grounded and aerial running seem to be justified (Fig. 7A). For the virtual leg, the numbers can be described by the same regression with respect to the Froude speed (Fig. 7B). Despite the fact that all regressions (see Fig. 7 caption) were highly significantly different from 0, the dependence on speed was much more prominent for the axial work component.

During steady-state aerial running with no net change in speed, it was expected that the total work of the virtual leg, i.e. the sum of its axial and tangential work, would vanish. The subdivision into the leg's axial and tangential work components depended on the location of the COM. However, net total translational work as calculated from the ground reaction forces, including double support, was independent of the actual placement of the COM within the body and of the leg models. In our experiments, total work, as obtained from the sum of the axial and tangential work of the virtual leg during contact, was proportional to the horizontal work on the COM with a slope that was not significantly different (P=0.241) from 1: ($W_{ax,COM}$+$W_{tan,COM}$) [mgl_{COM0}]=(0.014±0.003s.e.)+(1.112±0.095 s.e.)$W_{hor,COM}$ [mgl_{COM0}]; r^2=0.76; P<0.001; n=96. During most of the aerial running trials, the animal did work, especially by accelerating (mean acceleration during contact <0.08 [g]; see Materials and Methods).

For the effective and virtual legs, the resulting values extrapolated (index: ∼) towards the steady state were not significant for aerial running (Table 2). In addition, tangential work was not significant for the virtual leg during grounded running; it slightly differed from zero for the axial component of the virtual leg. The corrected axial work indicated absorption in the axial effective leg and net work in the tangential effective leg during grounded running.

For the grand means (N=96; across grounded and aerial running), this gave: $W_{ax,COM\sim}$=(−0.019±0.011s.e.) [mgl_{COM0}] for the axial component and $W_{tan,COM\sim}$=(0.013±0.009s.e.) [mgl_{COM0}] for the tangential component, both being not significantly different from zero (P>0.08). Only horizontal translational work contributed significantly (P<0.007) to this prediction, whereas contributions of the vertical work were not significant (P>0.4). However, for the effective leg, the extrapolated values for the grand means of axial work $W_{ax,hip\sim}$=(−0.096±0.016s.e.) [mgl_{hip0}] and tangential work $W_{tan,hip\sim}$=(0.139±0.013s.e.) [mgl_{hip0}] were different. Values differed significantly (P<0.001) from zero and both horizontal and vertical translational work components contributed significantly (P<0.007) to the extrapolation. The shift of the hip away from the COM caused absorption in the axial component and net positive work in the tangential component of the leg. The fact that the leg work did not add up to zero was due to the fact that the work of the effective leg ignored the considerable amount of work $W_{int\sim}$ of retracting the hip with respect to the COM (Fig. 1C). Ignoring the minor contributions owing to rotation, the latter could be estimated as $W_{int\sim}$=(−0.051±0.006s.e.) [mgl_{hip0}]. The sum of the relative hip work and work of the effective leg resulted in $W_{tot\sim}$=(−0.008±0.012s.e.) [mgl_{hip0}] being not different from zero (P=0.507), with significant (P<0.001) dependence on horizontal work.

DISCUSSION

During both grounded and aerial running, macaques trained for bipedal walking used the VPP strategy. The elevation of the VPP above the COM decreased with speed. Deviations from pure axial loading as described by the SLIP model were small during aerial running, but increased with decreasing speed. The properties of the effective leg significantly (P<0.001) differed from those of the virtual leg, supporting the effect of hip placement. Similar to birds, the posterior placement of the macaque hip caused energy loss in the axial direction. Much smaller losses were also observed for the axial virtual leg; the latter was compensated by corresponding tangential work. By contrast, the higher losses for the effective leg were more than compensated by tangential work. The corresponding energy gap was filled by work on the hip with respect to the COM. As in large ostriches (Rubenson et al., 2004), the transition from grounded to aerial running took place without abrupt transitions in mechanical parameters.

VPP control

During grounded and aerial running in macaques, the vector of the ground reaction force is directed to a point above the COM. Despite the fact that even trained macaques are only facultative bipedal animals, they generate a VPP strategy facilitating control of the rotatory momentum of the system. The height of the VPP observed in the macaque at low speeds exceeds the values estimated for humans {at a Froude speed of 0.34 and 0.5 [$\sqrt{(gl_{hip0})}$], VPP–height ratio=($\hat{z}_{VPP,mac}$ / $\hat{z}_{VPP,hum}$)=4.5 (Maus et al., 2010) as well as 2.7 and 1.9 for upright and bent postures, respectively (Müller et al., 2017)}. The VPP heights observed in quails are lower at low speeds and higher at high speeds at {Froude speeds of 0.31, 0.53 and 1.00 [$\sqrt{(gl_{hip0})}$]: VPP–height ratio=($\hat{z}_{VPP,mac}$ / $\hat{z}_{VPP,quail}$)=1.71, 1.02 and 0.39, respectively (Andrada et al., 2014)}. In contrast to quails, macaques strongly reduce this height once they reach aerial running speed. With vanishing double support, increasing impacts and almost upright posture, high VPP heights may lead to large oscillations. In general, how VPP control is achieved remains unclear. For macaques, the VPP control scheme, which probably

Journal of Experimental Biology (2018) 221, jeb178897. doi:10.1242/jeb.178897

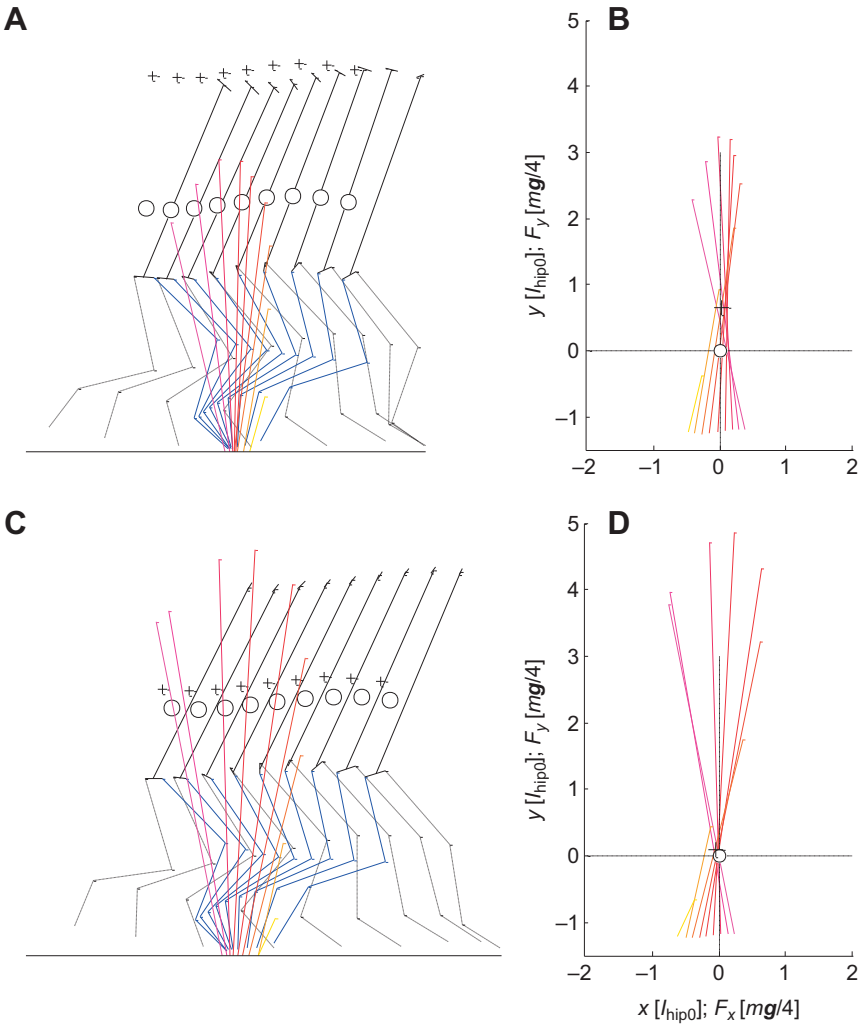

Fig. 3. Kinematics and ground reaction forces. (A,C) Sagittal projection of stick figures with ground reaction forces in grounded (A) and aerial running (C). Ground reaction forces with respect to the COM are also presented (B and D, respectively). Circles, COM; crosses, VPP. Left: scale of the floor lines: A, 0.753 m; C, 0.884 m. Force: 2 [***mg***]. The vectors of the ground reaction forces change from magenta to yellow with time. Single trials of Ku. (A,B) Speed: 1.20 m s^{-1}; duty factor: 0.63; t_c: 0.425 s; l_{hip0}=386 mm. (C,D) Speed: 2.11 m s^{-1}; duty factor: 0.48; t_c: 0.235 s; l_{hip0}=392 mm.

developed to facilitate quadrupedal locomotion, is probably adapted during training or the facilitating anatomical conditions are still available despite the postural change**.**

Global parameters

For the virtual leg, tangential as well as axial visco-elastic contributions were only minor. Owing to the posterior hip placement, mean retractive moments at the hip were observed. In the axial direction, the leg absorbs energy during grounded running. At higher speeds, the axial leg did work in our sample. Stiffness has a slight tendency to increase with speed, whereas damping decreases when reaching negative values at higher speeds of locomotion.

In reviewing the literature, it is necessary to be aware of the influence of the definition of reference leg length (l_0, see Materials and Methods). In macaques during grounded running, the leg lengths at touchdown and takeoff hardly differ (Figs 2C and 5, left). During aerial running, the change is of the order of ±0.05 [l_0], with a shorter leg at touchdown than at takeoff. Using touchdown length as a reference for the calculation, a damping of 1 would increase to 1.03 and a stiffness of 15 would increase to 16.6. The reduction of stiffness (Table 2) obtained during aerial compared with grounded running for the virtual leg would therefore vanish. The corresponding stiffness would then describe the value observed during the stiffer amortization phase (see Fig. 5, left).

All parameters marked with the suffix COM depend on the position of the COM, especially in the direction of locomotion. It was necessary to correct our estimates from cadaver values (see Materials and Methods). A reduction of the distance by 5% (ca. 3 mm) alters the mean values describing the kinematics presented in Table 1 significantly, but by less than 2%. The significant differences (Δ) on lumped parameters and work (Table 2; grounded running and aerial running) are Δk_{COM}=−0.141 and −0.184; ΔD_{COM}=−0.072 and −0.067; $\Delta W_{ax,COM}$=0.004 and 0.005; $\Delta W_{tan,COM}$=−0.004 and −0.005, repectively.

Stiffness

The stiffness of the macaque virtual leg was lower than comparable estimates for human walkers and aerial runners. For Froude speeds ranging from 0.17 to 1.22 (normalized to standing leg length l_{st0} and body weight), the human values range from 23 to 25 [mg/l_{st0}] for aerial running, and are higher for walking: 32 [mg/l_{st0}] (Lipfert et al., 2012). Because of the longer distance between the COP and the COM, these values can be considered lower bounds. Taking the initial length and a rough estimate of the COM height into account, the stiffness value documented by Lipfert et al. (2012) for aerial running shifts to a value of 31 [mg/l_{COM0}]. Taking the values for aerial running as reference, the stiffness estimated for the virtual leg of macaques during grounded and aerial running {17 [mg/l_{COM0}]} was 55% the human values. During grounded and aerial running,

Journal of Experimental Biology (2018) 221, jeb178897. doi:10.1242/jeb.178897

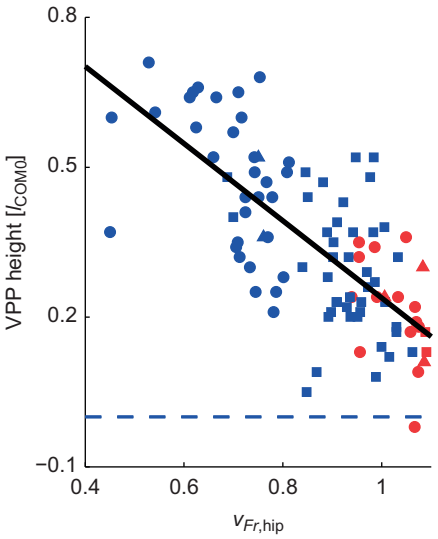

Fig. 4. Change in the VPP height with Froude speed ($v_{Fr,hip}$). Blue: grounded running; red: aerial running; Ku: circles; Fu: squares; Po: triangles. Regression: VPP height [l_{COM0}]=(1.01±0.07s.e.)+v_{Fr}·(−0.78±0.08s.e.); r^2=0.51; P=2E−16; n=96.

the macaques achieved a higher compliance. Future efforts are needed to standardize estimations. Here, we adhere to the notion that the virtual stiffness observed in macaques borders on the lower end of the values observed for human aerial runners. The fact that the dependency on speed is only weak in macaques is supported by corresponding observations in humans (Lipfert et al., 2012). For small birds, the stiffness values are lower. For the virtual leg of quails, the mean values are 5.8, 5.0 and 6.2 [mg/l_{COM0}] in walking, grounded and aerial running, respectively, corresponding to Froude speeds of 0.37, 0.45 and 0.60, respectively (Andrada et al., 2013). The virtual legs operate quasi-elastically, and l_0 has been chosen as the mean between the touchdown and takeoff lengths in this estimation. The virtual leg lengthens by less than 10% of l_{COM0}. For larger birds (e.g. pheasant, guinea fowl, turkey and ostrich), the stiffness values (11–15 [mg/l_{COM0}]; Müller et al., 2016) approach those observed for macaques from the lower side. The stiffness of the macaque's virtual leg is intermediate between those observed for humans and birds; however, it is close to observations in other animals (Blickhan and Full, 1993). We argue below that the lower stiffness values observed in macaques and birds as compared with humans are sufficient to explain the preference of the former species for grounded running.

The stiffness of the macaque's effective leg was significantly lower than that of the virtual leg (P<0.001). To a large extent, this was the result of the different lengths (normalization). The ratio of the stiffness values was 1.5 for walking and 1.42 for aerial running, and the ratio of the leg lengths was 1.32. The remaining deviation was a result of the relative movements of the hip with respect to the COM (see Fig. 1C and Results, 'Work', above). In a recent study, we investigated the influence of posture during human walking {Froude speeds from 0.42 to 0.65 [$\sqrt{(gl_{hip0})}$]} on global parameters (Aminiaghdam et al., 2017). Stiffness values (21.8± 8.18s.d.) [mg/l_{hip0}] did not depend on posture (P>0.14; Fig. 8). Owing to the pronograde posture and hip placement, the effective legs of birds, and, in particular, of the quail, shorten considerably (up to 26% of the mean touchdown and takeoff lengths during walking). In a corresponding publication (Andrada et al., 2014), stiffness was normalized using the touchdown length l_{hipTD}, and this

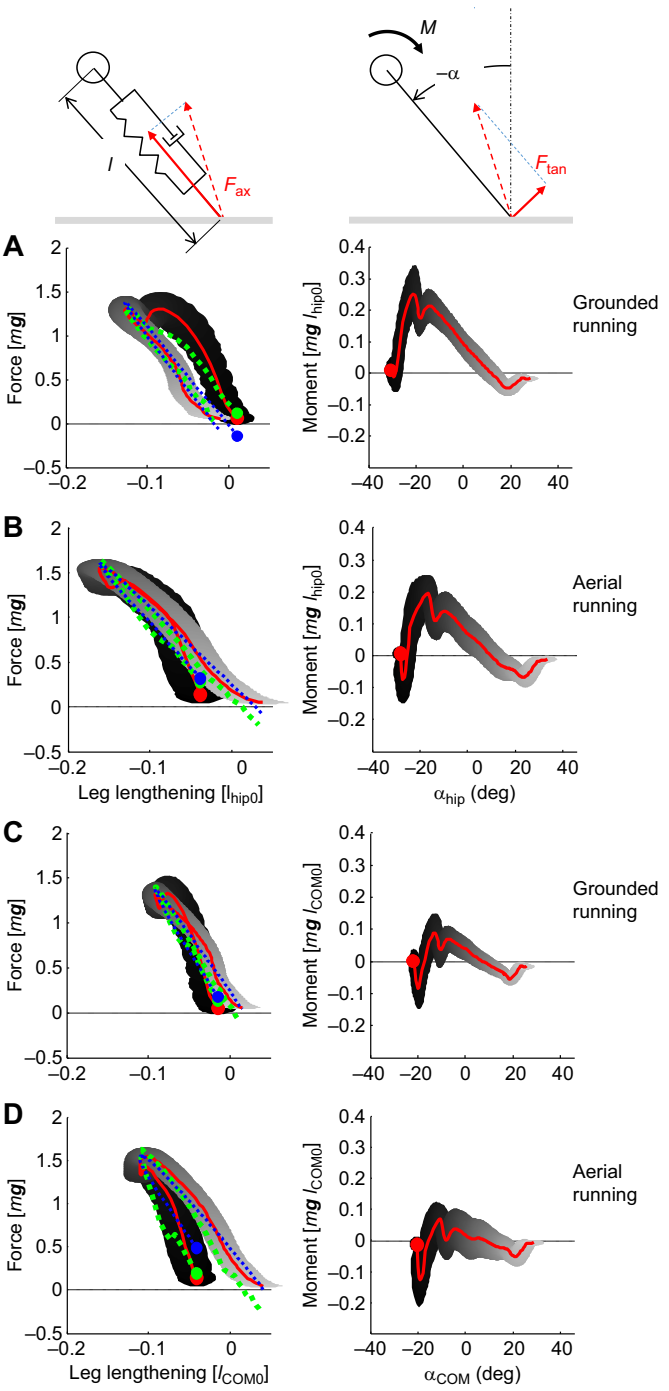

Fig. 5. Mean axial and tangential loops for the effective leg and virtual leg. (A,B) Effective leg; (C,D) virtual leg. Left: axial force (F_{ax}) versus leg shortening [force $F(l–l_0)$, where l_0 refers to l_{hip0} and l_{COM0}, respectively]. Green dashed lines: corresponding mean curves of the fittings using the Voigt model. Blue dashed lines: means of the fittings based on the Maxwell model. Right: moment (M) generated by the tangential component of the ground reaction force versus rotation of the effective and virtual legs, respectively. Red lines: mean values; shading from black at touchdown to light gray at takeoff: ±s.d. Circles indicate touchdown. F_{tan}, tangential force.

must be taken into account in the comparison (see Materials and Methods). The corrected stiffness calculated for the effective leg of the quail during walking, grounded running and aerial running at Froude speeds of 0.33, 0.58 and 0.93 [$\sqrt{(gl_{hip0})}$], respectively, were 6.12, 8.25 and 8.64 [mg/l_{hip0}], respectively. These values were only

Journal of Experimental Biology (2018) 221, jeb178897. doi:10.1242/jeb.178897

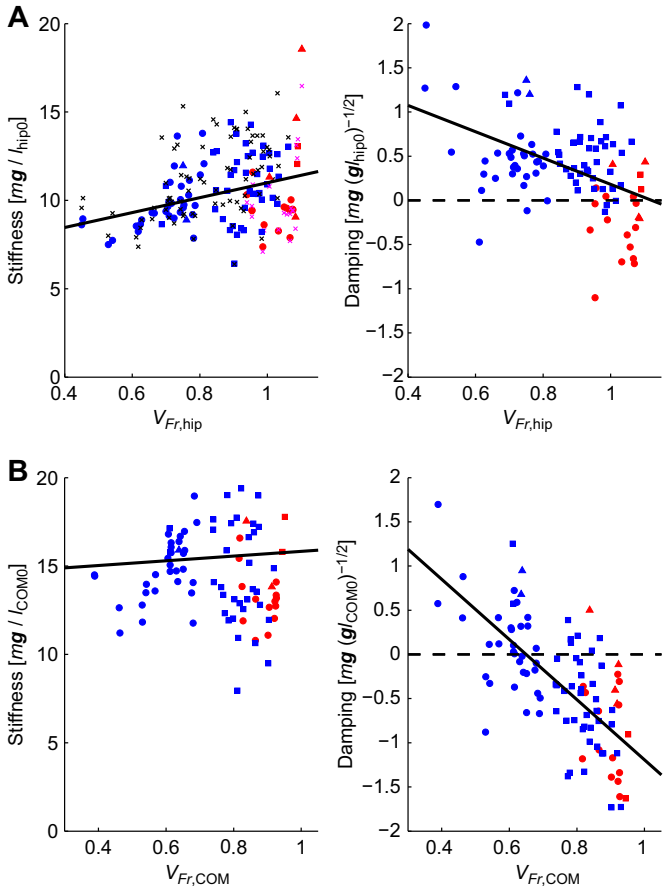

Fig. 6. Dependence of dimensionless stiffness and damping coefficients on Froude speed during grounded running (blue symbols) and aerial running (red symbols) for the effective leg and virtual leg. (A) Effective leg (hip-COP); (B) virtual leg (COM-COP).The regressions (black lines) were obtained for the whole dataset. Crosses in A (left): dimensionless stiffness as obtained from peak force to spring compression ratios. Ku: circles; Fu: squares; Po: triangles. Regressions for the effective leg (means±s.e.; stiffness: *k*; damping: *D*): $k\ [mg/l_{hip0}]=(6.77\pm1.10)+(4.23\pm1.25)v_{Fr,hip}$, $r^2=0.11$, $P=0.001$; $D\ [mg/l_{hip0}]=(1.67\pm0.26)+(-1.49\pm0.29)v_{Fr,hip}$, $r^2=0.21$, $P=2E-6$. Regressions for the virtual leg: $k\ [mg/l_{COM0}]=(13.87\pm2.00)+(1.88\pm2.26)v_{Fr,COM}$, $r^2=0.007$, $P=0.608$; $D\ [mg/l_{COM0}]=(2.18\pm0.31)+(-2.91\pm0.35)v_{Fr,COM}$, $r^2=0.42$, $P=9E-14$.

slightly below those of the macaques (Fig. 8). Clearly, the stiffness of human walkers is almost double that observed in the macaque and quail, and this does not appear to be a size effect. Compared with primates, humans have developed a rather stiff-legged bipedal gait (Schmitt, 1999, 2003).

Alexander (1989; p. 1200) defined as follows: 'A gait is a pattern of locomotion characteristic of a limited range of speeds described by quantities of which one or more change discontinuously at transitions to other gaits'. Stiffness, similar to other parameters (Ogihara et al., 2018), did not show discontinuous change at the transition from grounded to aerial running. In contrast to the general tendency (Fig. 6, left), the mean stiffness of the virtual leg for aerial running was slightly below that estimated for grounded running. This would parallel the decrease of stiffness observed in the transition from human to aerial running. Aerial running occurs in the macaque at Froude speeds above about 0.8 [$\sqrt{(gl_{COM0})}$] (Figs 6B and 7B). Below this speed, the generated momentum is not sufficient to allow for aerial phases. The discontinuous transition from walking to aerial running observed in human locomotion is the result of a corresponding discontinuous change in leg properties.

Damping

The effective leg of the macaque shows a significant contribution from damping. This was expected because of the posterior placement of the hip with respect to the COM. Surprisingly, despite correcting for acceleration, significant negative damping for the virtual leg remained. In other words, whereas the effective leg showed net shortening from touchdown to takeoff, the virtual leg showed net lengthening. The tangential component is included in the discussion on leg work below.

Currently, damping coefficients are available only for small birds (Andrada et al., 2014) and humans walking with a bent trunk (Aminiaghdam et al., 2017). The latter study used a series visco-elastic model (Maxwell model) to calculate damping coefficients. Despite the fact that this model sometimes results in a better description (see Fig. 5, left) than the parallel arrangement of spring and damper (Voigt model), we do not consider it useful because of the scatter of our data. In the purely elastic case, the serial damping in the Maxwell model has to approach infinity. Correspondingly, because of this non-linear behavior, any mean value including quasi-elastic cases becomes meaningless. Recalculation of the damping of the human trials based on the Voigt model revealed a strong and highly significant ($P<0.001$) dependency on posture {damping was (1.00±2.55s.d.), 3.14±2.23s.d.), (3.55±2.36s.d.) and (4.96±3.26s.d.) [$mg/\sqrt{(gl_{hip0})}$] for upright, 30 deg, 60 deg and maximum pronograde posture, respectively (n=70, 64, 68 and 74)}. The values measured for upright human walking were close to those obtained for the macaque during grounded running. However, those observed in the case of maximum bending were much larger than those observed for the walking quail (see below).

The damping values for the walking, grounded running and aerial running of the quail {Froude speeds of 0.33, 0.57 and 1.04 [$\sqrt{(l_{hip0}g)}$], respectively} were 3.77, 3.49 and 2.1 [$mg/\sqrt{(l_{hip0}g)}$] higher than those calculated for the macaque (Andrada et al., 2014). The horizontal displacement of the macaque's hip was about one-third that observed for the quail, and a corresponding ratio may be expected in the damping; this is valid for lower speeds. The corrected values obtained for aerial running were not significantly different from zero. We therefore conclude that the posterior displacement of the hip with respect to the COM induces damping in the macaque leg.

The systematics with respect to the speed, size, gait and posture of these values across the available data appear to be limited (Fig. 8). Stiffness of the effective leg as observed during human walking was high, and the trend owing to size was not sufficient to explain this difference. The low damping observed in the macaque may be related to the combined effect of an almost upright posture and high speeds. Above all, variance was found between subjects. For the macaque, we expected corresponding variation, as the animals differed with respect to age and training. To a large extent, the considerable variance found in human walkers can be attributed to different preferred speeds. However, interindividual variance requires further attention. Minimization of losses by quasi-elastic operation of the leg is only relevant for species exploring steady-state locomotion. For most species, unsteady locomotion is the rule. This also seems to be case for the macaque. Based on the data available, bipedal locomotion in macaques is not hampered by extraordinary losses with respect to operation of the effective leg, making the exploration of resonances useful (see below).

Journal of Experimental Biology (2018) 221, jeb178897. doi:10.1242/jeb.178897

Table 2. Stiffness (k), damping (D), axial work (W_{ax}) and tangential work (W_{tan}) of the effective (hip) and virtual (COM) legs during grounded running and aerial running

Variables		Grounded running (mean±s.d.)	*P* (/0)	Aerial running (mean±s.d.)	*P* (/0)	*P* (GR/R)
k_{hip}	mg/l_{hip0}	10.5±1.9	0.000	10.5±2.6	0.003	1.000
k_{COM}	mg/l_{COM0}	15.7±3.3	0.000	14.9±3.9	0.003	0.003
D_{hip}	$mg/(\sqrt{g}l_{hip0})$	0.52±0.40	0.003	−0.20±0.41	0.105	0.000
D_{COM}	$mg/(\sqrt{g}l_{COM0})$	−0.23±0.66	0.000	−0.84±0.63	0.000	0.000
$W_{ax,hip}$	mg/l_{hip0}	−0.058±0.036	0.000	0.032±0.059	0.066	0.000
$W_{ax,COM}$	mg/l_{COM0}	0.011±0.066	0.015	0.066±0.050	0.000	0.000
$W_{tan,hip}$	mg/l_{hip0}	0.090±0.033	0.000	0.045±0.040	0.000	0.000
$W_{tan,COM}$	mg/l_{COM0}	0.009±0.025	0.000	−0.006±0.034	0.093	0.000
$k_{hip\sim}$	mg/l_{hip0}	11.2±6.2	0.000	9.1±12.1	0.012	0.509
$k_{COM\sim}$	mg/l_{COM0}	17.0±10.2	0.000	14.1±16.6	0.000	0.660
$D_{hip\sim}$	$mg/\sqrt{(gl_{hip0})}$	0.97±1.16	0.000	0.25±1.15	1.000	0.000
$D_{COM\sim}$	$mg/\sqrt{(gl_{COM0})}$	−0.58±0.99	0.033	0.15±2.42	1.000	0.000
$W_{ax,hip\sim}$	mg/l_{hip0}	−0.093±0.113	0.000	−0.029±0.188	1.000	0.000
$W_{ax,COM\sim}$	mg/l_{COM0}	0.028±0.096	0.036	−0.013±0.148	1.000	0.000
$W_{tan,hip\sim}$	mg/l_{hip0}	0.137±0.096	0.000	0.075±0.192	0.303	0.000
$W_{tan,COM\sim}$	mg/l_{COM0}	0.009±0.070	0.070	0.011±0.170	1.000	0.268

∼: extrapolated towards zero translational work. /0: with respect to 0; GR/R: grounded versus aerial running.

Normalizing the contact time (t_c) to cycle frequency (ω_{COM}) of the spring–mass system allows us to evaluate modes of oscillations (Geyer et al., 2006) and the influence of damping on the oscillations. The double-humped force pattern typical for pendular walking can be considered a resonance exploring the 1.5-fold of the sinusoidal resonance [$\sin(t')$, with $0 \leq t' \leq 3\pi$]. In contrast, for grounded and

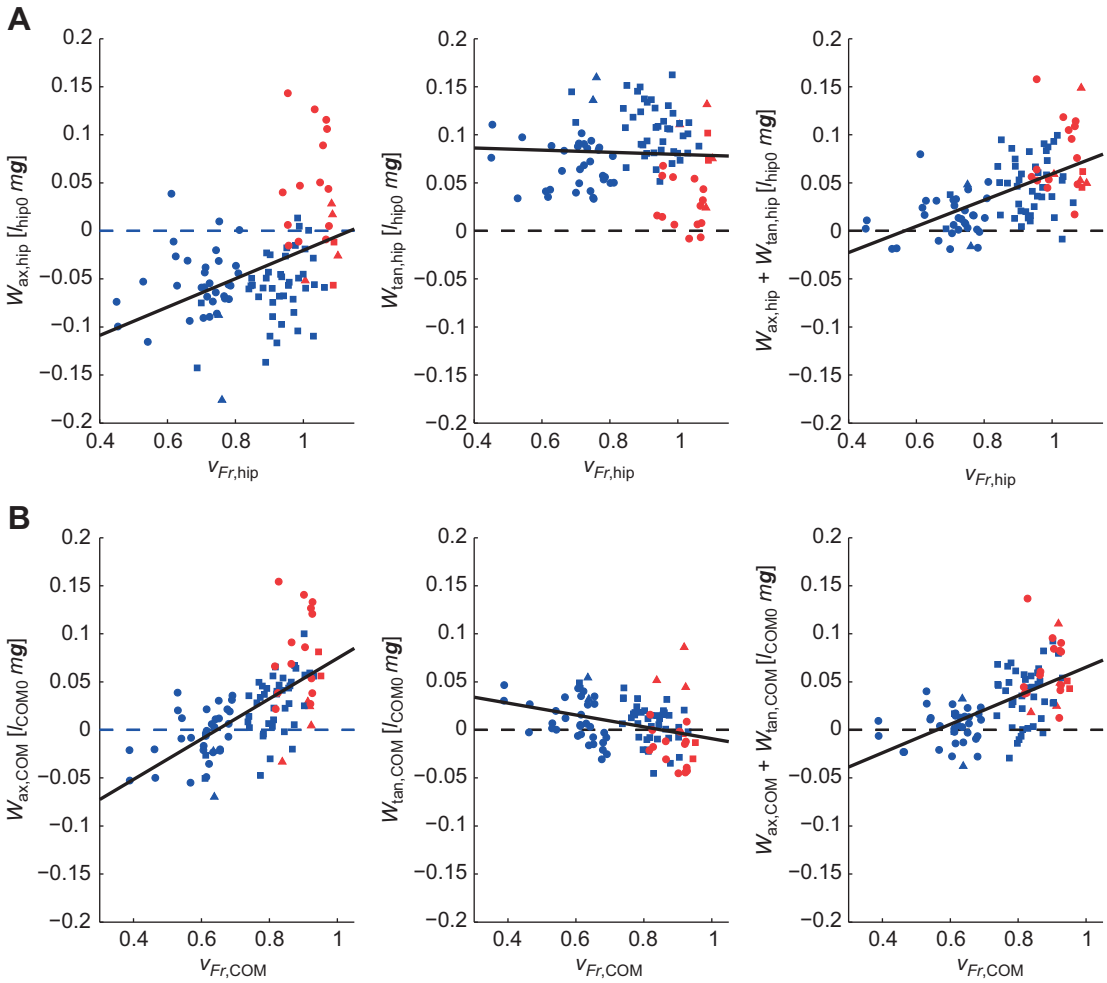

Fig. 7. Axial work (left), tangential work (middle) and their sum (right) plotted against Froude speed for the effective leg and virtual leg. (A) Effective leg (hip-COP); (B) virtual leg (COM-COP). Regressions (means±s.e.): $W_{ax,hip}$ [mgl_{hip0}]=(−0.168±0.030)+(0.148±0.034)$v_{Fr,hip}$, r^2=0.17, P=3E−5; $W_{tan,hip}$ [mgl_{hip0}]=(0.091±0.023)+(−0.011±0.026)$v_{Fr,hip}$, r^2=0.002, P=0.668; $W_{tot,hip}$ [mgl_{hip0}]=(−0.077±0.018)+(0.137±0.020)$v_{Fr,hip}$, r^2=0.33, P=9E−10; $W_{ax,COM}$ [mgl_{COM0}]=(0.136±0.019)+(0.210±0.025)$v_{Fr,COM}$, r^2=0.42, P=8E−13;$W_{tan,COM}$ [mgl_{COM0}]=(0.052±0.014)+(−0.062±0.018)$v_{Fr,COM}$, r^2=0.11, P=9E−4;$W_{tot,COM}$ [mgl_{COM0}]=(−0.083±0.016)+(0.148±0.021)$v_{Fr,COM}$, r^2=0.36, P=1E−10; N=96. For markers, see Fig. 6.

Journal of Experimental Biology (2018) 221, jeb178897. doi:10.1242/jeb.178897

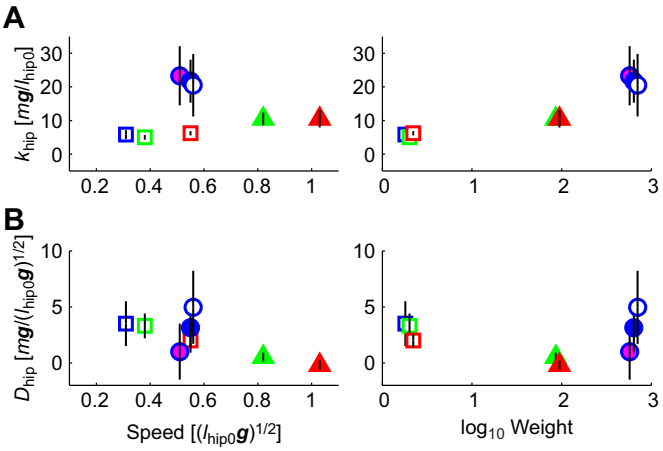

Fig. 8. Stiffness and damping of the effective leg for quails (squares), macaques (triangles) and humans (circles). (A) Stiffness; (B) damping. Weight was measured in newtons. Whiskers: ±s.d. Gait, edge color: walking – blue; grounded running – green; aerial running – red. Posture, face color: open – pronograde; filled –30 deg; magenta – upright.

aerial running, single-humped force patterns are typical, with force patterns exploring resonances from 1- to 0.5-fold of the period [from $-\cos(t')$ with $0 \leq t' \leq 2\pi$ to $\sin(t')$, with $0 \leq t' \leq \pi$]. For the macaque, the mean $\hat{t}_c = t_c / \omega_{COM}$ is (5.17±1.09s.d.) [$1/\omega_{COM}$] or 1.64π for grounded running and (3.92±0.48s.d.) [$1/\omega_{COM}$] or 1.24π for aerial running.

Contact times normalized to the cycle frequency observed in the quail {7.92, 5.41 and 3.13 [$1/\omega_{COM0}$], or 2.52π, 1.72π and 1.00π for walking, grounded running and aerial running, respectively} were similar to those observed for the macaque for similar gaits. For walking, the contact time exceeded the period of the system (>2π).

In human walking (Aminiaghdam et al., 2017), the contact times normalized to the cycle frequency, (8.76±1.78s.d.) [$1/\omega_{COM}$] or 2.79π, were clearly above the period of the virtual leg; this changed only slightly with posture. For macaques, lower stiffness makes a slow running gait preferable. The preference for grounded running over walking in macaques and birds can be attributed to leg compliance. Generation of a double-humped force pattern requires more leg stiffness.

Both macaques and humans operate far from critical damping. The aperiodic limit, i.e. when oscillations are suppressed, would be reached for $\hat{D}$ [$mg/\sqrt{(l_0 g)}$]=$2\sqrt{(\hat{k}}$ [mg/l_0]). In both macaques and humans, upright locomotion damping approaches only 20% of this limit. However, human walking with maximal bent postures reaches 55% and quail walkers reach 73%, indicating dramatic losses and thus making the exploration of leg resonances inefficient. In the macaque, the exploration of resonances is helpful; they use single-humped force patterns typical for grounded and aerial running. Our data were recorded while animals moved along a short track. Although our animals are certainly not long-distance runners, they tried to cross the track quickly. Our complete dataset (Ogihara et al., 2018) does not contain a single trial which we could classify as walking. In earlier studies (Kimura et al., 1983; Ogihara et al., 2010), within a range of observed speeds from 0.5 to 1.7 m s^{-1}, Japanese macaques trained for bipedal locomotion did not show the double-humped force pattern typical for walking in birds and humans. Macaques seem to avoid or not be able to walk bipedally because of the compliant nature of their legs. Leg compliance may also contribute to the inefficient use of pendular mechanisms during quadrupedal locomotion (Ogihara et al., 2012).

Work

Work allows us to evaluate the net losses or gains independent of the model used to describe the visco-elastic leg properties. The expectation that without any correction the contributions of the axial and tangential leg would compensate was not fulfilled for either the effective leg or the virtual leg. As the leg work represents the only source for changes in the energy of the COM, the axial and tangential work of the virtual leg should compensate**.** This forced us to check for bias in our data (see Materials and Methods, and Results, 'Work', above, and the introduced extrapolations). The correction used across the entire sample gave satisfying results with respect to the global means, including both grounded and aerial running. Among the gaits, only the mean $W_{ax,COM\sim}$ had a small but significant value. The differences observed for the damping coefficient between the effective and virtual legs were mirrored by the corresponding differences of axial losses. The grand means of the work in the effective leg differed from those of the virtual leg by $\Delta W_{ax\sim}$=−0.091 [mgl_{COM0}] for the axial work and $\Delta W_{tan\sim}$=0.091 [mgl_{COM0}] for the tangential work. To elucidate the magnitude of this work, this corresponds to the macaque lifting its own weight by about 4 cm, which confirms the interpretation of the identified visco-elastic losses in the effective leg. The posterior placement of the hip with respect to the COM introduces considerable visco-elastic losses in the axial effective leg. The axial and tangential components of the work of the effective leg do not add up to zero. This energy gap can largely be attributed to the work of the hip with respect to the COM. Some of this may be the result of hip rotation, as has been observed in chimpanzees (O'Neill et al., 2015).

The losses enforced by hip placement (visco-elastic), the VPP control scheme (moment arms) and the compliant gait (bent knees) may make bipedal locomotion more expensive than quadrupedal locomotion in macaques (Nakatsukasa et al., 2006) and bipedal locomotion in humans. In birds, it seems that the additional cost can be reduced by an anatomical trick, i.e. placing the knee close to the COM (Blickhan et al., 2015). However, more importantly, results from ongoing research (E.A.) suggest that the cost may pay off by facilitating stabilization; this may not be the case for the slightly flexed posture used by the macaques. The large variation visible in our data (see Figs 6 and 7) can be taken as evidence that macaques may not be able to take advantage of local system stability. Macaques may be able to stabilize the trunk, but at the cost of slight acceleration (results of preliminary numerical simulations; E.A.) or, as in humans, they may balance the upright trunk like an inverted pendulum (Müller et al., 2017). In that case, they would be forced to stabilize their posture actively, resulting in additional costs. Nevertheless, by using grounded running, the macaque's locomotor system allows for an exploration of system resonances during bipedal locomotion, even with compliant legs. However, the absence of stiff-legged walking typical for human locomotion may constitute an energetic disadvantage.

Acknowledgements

Data for human walking at different postures were provided by Soran Aminiaghdam and Roy Müller, Friedrich-Schiller University, Jena, Germany. We wish to express our gratitude to the staff of the Suo Monkey Performance Association for their generous collaboration in these experiments. Thanks are also owed to Naoki Kitagawa, Kohta Ito, Hideki Oku and Mizuki Tani from Keio University, Yokohama, Japan, and to Martin Götze at Friedrich-Schiller University, Jena, Germany, for helping us with the data collection. We also thank Ryoji Hayakawa, ArchiveTips, Inc., Tokyo, Japan, for support and preprocessing with Qualisys. Thanks are also due to Dr Roy Müller for reading an early draft of the manuscript.

Competing interests

The authors declare no competing or financial interests.

Author contributions

Conceptualization: R.B., N.O.; Methodology: E.A., N.O.; Software: R.B.; Formal analysis: R.B.; Investigation: R.B., E.H., N.O.; Resources: E.H., N.O.; Data curation: N.O.; Writing - original draft: R.B.; Writing - review & editing: E.A., N.O.; Supervision: N.O.; Project administration: N.O.; Funding acquisition: N.O.

Funding

This work was supported by a research initiation grant of the Deutsche Forschungsgemeinschaft to R.B. (BL 236/28-1), Grants-in-Aid for Scientific Research (#10252610, #17H01452) from the Japan Society for the Promotion of Science, a Cooperative Research Fund of the Primate Research Institute, Kyoto University to N.O. and a guest professorship to R.B. from Keio University.

Data availability

Dynamic and kinematic data are available from figshare: https://figshare.com/s/10691e3dc6e9612017ee. Software for data processing are available on request from the corresponding author (reinhard.blickhan@uni-jena.de).

References

Alexander, R. M. (1989). Optimization and gaits in the locomotion of vertebrates. *Physiol. Rev.* **69**, 1199-1227.

Aminiaghdam, S., Rode, C., Müller, R. and Blickhan, R. (2017). Increasing trunk flexion transforms human leg function into that of birds despite different leg morphology. *J. Exp. Biol.* **220**, 478-486.

Andrada, E., Rode, C. and Blickhan, R. (2013). Grounded running in quails: Simulations indicate benefits of observed fixed aperture angle between legs before touch-down. *J. Theor. Biol.* **335**, 97-107.

Andrada, E., Rode, C., Sutedja, Y., Nyakatura, J. A. and Blickhan, R. (2014). Trunk orientation causes asymmetries in leg function in small bird terrestrial locomotion. *Proc. Roy. Soc. B.* **281**, 20141405.

Blickhan, R. (1989). The spring-mass model for running and hopping. *J. Biomech.* **22**, 1217-1227.

Blickhan, R. and Full, R. J. (1993). Similarity in multilegged locomotion: Bouncing like a monopode. *J. Comp. Physiol., A* **173**, 509-517.

Blickhan, R., Andrada, E., Müller, R., Rode, C. and Ogihara, N. (2015). Positioning the hip with respect to the COM: Consequences for leg operation. *J. Theor. Biol.* **382**, 187-197.

Geyer, H., Seyfarth, A. and Blickhan, R. (2006). Compliant leg behaviour explains basic dynamics of walking and running. *Proc. Roy. Soc. B.* **273**, 2861-2867.

Hayama, S., Nakatsukasa, M. and Kunimatsu, Y. (1992). Monkey performance: the development of bipedalism in trained Japanes monkeys. *Kaibogaku Zasshi. J. Anat.* **67**, 169-185.

Kimura, T., Okada, M., Yamazaki, N. and Ishida, H. (1983). Speed of the bipedal gaits of man and nonhuman primates. *Ann. Sci. Nat., Zool.* **5**, 145-158.

Lipfert, S. W., Günther, M., Renjewski, D., Grimmer, S. and Seyfarth, A. (2012). A model-experiment comparison of system dynamics for human walking and running. *J. Theor. Biol.* **292**, 11-17.

Maus, H. M., Lipfert, S. W., Gross, M., Rummel, J. and Seyfarth, A. (2010). Upright human gait did not provide a major mechanical challenge for our ancestors. *Nat. Com.* **1**, 70.

Müller, R., Birn-Jeffery, A. V. and Blum, Y. (2016). Human and avian running on uneven ground: a model-based comparison. *J. R. Soc. Interface* **13**, 20160529.

Müller, R., Rode, C., Aminiaghdam, S., Vielemeyer, J. and Blickhan, R. (2017). Force direction patterns promote whole body stability even in hip-flexed walking, but not upper body stability in human upright walking. *Proc. Roy. Soc. A* **473**, 20170404.

Nakatsukasa, M. and Hayama, S. (1991). Structural strength of the femur of bipedally trained monkey. *J. Anthropological Soc. Nippon* **99**, 289-296.

Nakatsukasa, M., Hirasaki, E. and Ogihara, N. (2006). Energy expenditure of bipedal walking is higher than that of quadrupedal walking in Japanese macaques. *Am. J. Phys. Anthropol.* **131**, 33-37.

O'Neill, M. C., Lee, L.-F., Demes, B., Thompson, N. E., Larson, S. G., Stern, J. T., , Jr and Umberger, B. R. (2015). Three-dimensional kinematics of the pelvis and hind limbs in chimpanzee (*Pan troglodytes*) and human bipedal walking. *J. Hum. Evol.* **86**, 32-42.

Ogihara, N., Hirasaki, E., Kumakura, H. and Nakatsukasa, M. (2007). Ground-reaction-force profiles of bipedal walking in bipedally trained Japanese monkeys. *J. Hum. Evol.* **53**, 302-308.

Ogihara, N., Makishima, H., Aoi, S., Sugimoto, Y., Tsuchiya, K. and Nakatsukasa, M. (2009). Development of an anatomically based whole-body musculoskeletal model of the Japanese macaque (*Macaca fuscata*). *Am. J. Phys. Anthropol.* **139**, 323-338.

Ogihara, N., Makishima, H. and Nakatsukasa, M. (2010). Three-dimensional musculoskeletal kinematics during bipedal locomotion in the Japanese macaque, reconstructed based on an anatomical model-matching method. *J. Hum. Evol.* **58**, 252-261.

Ogihara, N., Aoi, S., Sugimoto, Y., Tsuchiya, K. and Nakatsukasa, M. (2011). Forward dynamic simulation of bipedal walking in the Japanese macaque: Investigation of causal relationships among limb kinematics, speed, and energetics of bipedal locomotion in a nonhuman primate. *Am. J. Phys. Anthropol.* **145**, 568-580.

Ogihara, N., Makishima, H., Hirasaki, E. and Nakatsukasa, M. (2012). Inefficient use of inverted pendulum mechanism during quadrupedal walking in the Japanese macaque. *Primates* **53**, 41-48.

Ogihara, N., Hirasaki, E., Andrada, E. and Blickhan, R. (2018). Bipedal gait versatility in the Japanese macaque (*Macaca fuscata*). *J. Hum. Evol.* **125**, 2-14.

Rubenson, J., Heliams, D. B., Lloyd, D. G. and Fournier, P. A. (2004). Gait selection in the ostrich: mechanical and metabolic characteristics of walking and running with and without an aerial phase. *Proc. Roy. Soc. B.* **271**, 1091-1099.

Schmitt, D. (1999). Compliant walking in primates. *J. Zool.* **248**, 149-160.

Schmitt, D. (2003). Insights into the evolution of human bipedalism from experimental studies of humans and other primates. *J. Exp. Biol.* **206**, 1437-1448.